Responses to Reviewer #1

We appreciate the reviewer's comments and suggestions on our manuscript. Our replies follow each of Reviewer's comments or suggestions. The revised text in our revised manuscript is highlighted in red.

Comments：

1. Lines 98-101: does "These data" refer to GODAS? Is atmospheric data just winds and geopotential? Please clarity.

Response: "These data" refer to Agro and GODAS data. Atmospheric data used in this study only includes winds and geopotential height. The related explorations are added in our revised manuscript (see lines 102 and 104 on page 6).

2. Line 104: This is not an energy equation, it is the heat equation. This needs to be corrected throughout.

Response: Corrected.

3. Line 117/118: dissipation is a subgridscale process. In general this term is not large, but the authors make no attempt to understand what process is important. It seems mostly likely to be entrainment in Fig. 4f, but some scaling estimate would be useful here. It could also be lateral eddy fluxes.

Response: As mentioned by the reviewer, the residual term, including the sub-grid scale process, is relatively large in our results, which may be due to the eddy-induced heat fluxes. Wunsch (1999) noted that eddy-induced heat fluxes are important relative to the total meridional heat fluxes in western boundary current regions of the North Atlantic and Pacific Oceans. Moreover, Qiu and Chen (2005) showed that the meridional eddy-induced heat fluxes over the subtropical North Pacific are both poleward for warm-core eddy detected in 11 Mar–3 Jun 2001 and cold-core eddy detected in 30 Dec 2001–24 Feb 2002. Accordingly, the poleward eddy-induced heat fluxes tend to transport the warm water from lower latitude to the subtropics, and benefit the warmer water there. These findings are consistent with our result that the residual term leads to the increasing SST over the NPSTF. Thus, the residual term

increasing the SST over the NPSTF is very likely due to the meridional eddy fluxes. However, it is still hard to confirm this process at this stage because the spatial and temporal resolutions of observation and reanalysis data used in study are relatively coarse. Thus, further exploration is needed when finer data becomes available to us. We add this discussion in our revised manuscript (see lines 366-380 on page 19).

4. Line 141: Show the region of interest on Fig.1.

Response: Fixed.

5. Line 146: define the winter and spring time period.

Response: The winter and spring time periods in this study are from December to February and from March to May, respectively, which are defined in Figure 1 (see lines 535-540 on page 27).

6. Line 147: I do not understand "maximum center expanding".

Response: The statement was revised to "The maximum center of ocean temperature gradients could expand from surface downward to the depth of 60 m." (see lines 150-152 on page 9).

7. Figure 2: The zonal velocity is surprisingly weak in the region of strongest SST gradient. Is this because salinity is density compensating?

Response: As mentioned by the reviewer, the relatively weak zonal velocity in the region of the strongest SST gradient may be due to the compensation of the salinity gradient. Figure S1 shows the latitude-depth section of the climatological mean zonal current velocity, ocean temperature (TEMP) gradient and salinity (SALT) gradient averaged from December to May. The ocean temperature gradient and salinity gradient are calculated by $-\partial TEMP/\partial y$ and $\partial SALT/\partial y$, respectively, in which the zonal velocity is positively correlated with both the ocean temperature gradient and salinity gradient. Accordingly, the zonal velocity is positive and strong around 20°N

where the ocean temperature gradient and salinity gradient are both positive and strong. However, the zonal velocity is positive but relatively weak over the 25°–30°N where the ocean temperature gradient is positively strong while the salinity gradient is negatively strong. Thus, the relatively weak zonal velocity over the 25°–30°N may be due to the compensation of the salinity gradient. We add this discussion in our revised manuscript (see lines 163-165 on page 9).

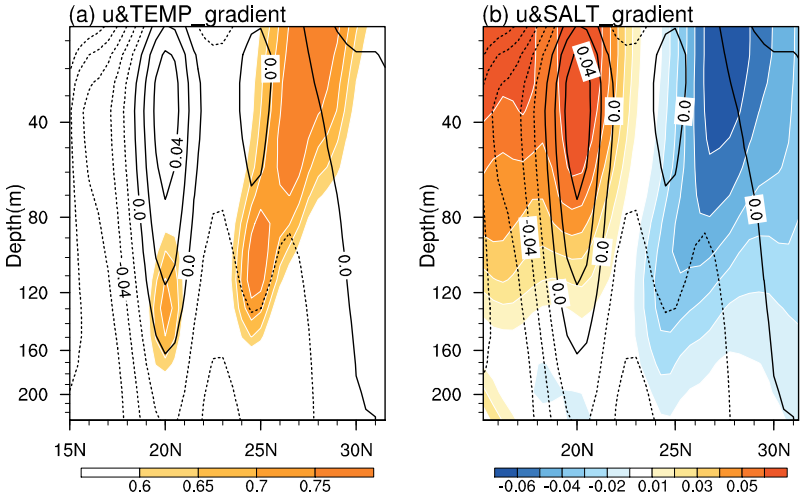

Figure S1. Latitude-depth section of the climatological zonal current velocity (black contour; units: m s^{-1}), superimposed with (a) ocean temperature gradient ($-\partial SST/\partial y$; shading; units: °C (100 km)$^{-1}$) and (b) ocean salinity gradient ($\partial SALT/\partial y$; shading; units: g (kg 100 km) $^{-1}$) zonally averaged over 140°E–170°W from December to May.

8. Line 151: Ecpect->Except

Response: Fixed.

9. Line 163: I do not see a significant southward shift from Sep to Feb. Similar for the "slightly migrates southward until March" comment.

Response: Qiu and Kawamura (2012) reported the NPSTF experiences the seasonally meridional shift. During the frontogenesis, the center of the NPSTF is around 28°N in December and migrates southward to 27°N in March. As mentioned by the reviewer, this 1° latitude shift from December to March may be not significant. However, the

meridional scale of the NPSTF is only approximately 6° latitudes (i.e., 24°–30°N), thus we consider that this southward shift is significant relative to its meridional scale.

10. Figure 3 and line 205: Why does the residual act to halt frontogenesis? Some ideas and order of magnitude estimates would be useful here. The NCAR model could provide the residual terms explicitly.

Response: Qiu and Chen (2005) found that winter and annual-average eddy-induced heat fluxes are both poleward over the subtropical North Pacific. Accordingly, the eddy-induced heat fluxes tend to transport the warm water from the lower latitudes to the subtropics, favoring the warm water in the subtropics. Our results are consistent with theirs that the residual term benefits the increasing SST over the NPSTF during the frontogenesis. Thus, the eddy-induced heat flux may play an important role in the residual term to increase the SST and to further halt the frontogenesis. However, it is still hard to confirm this process at this stage because the spatial and temporal resolutions of observation and reanalysis data used in study are relatively coarse. Our slab model diagnoses the SST only based on surface heat flux and fails to provide the residual term. Thus, further exploration is needed when finer data becomes available to us. We add this discussion in our revised manuscript (see lines 366-380 on page 19).

11. Lines 221, 224, 233: It seems that the findings up until this point are not new. Please clarify if I misunderstand.

Response: Although previous studies have demonstrated that both net heat flux and meridional temperature advection contribute to the NPSTF frontogenesis (Kazmin and Rienecker, 1996; Dinniman and Rienecker, 1999), relative importance of these two factors in the frontogenesis is not stated clearly. We further find that the net heat flux and meridional temperature advection play different roles in the different periods of the frontogenesis. Moreover, the role of the atmosphere in the frontogenesis is also explored. The atmosphere not only benefits the meridional temperature advection but also acts to transform dominant effect of the net heat flux to the joint contributions of

the meridional temperature advection and net heat flux. We clarify our conclusions in revised manuscript (see lines 16-19 on page 2 and 336-343 on page 17).

12. Figure 10 and discussion: I did not find this very surprising, but also not very useful.

Response: Figure 10 and the related discussion are no longer presented in our revised manuscript.

13. Line 329: I think of a slab ocean model as one that has no advection. However, this slab model has a horizontal advection (line 356/357) so I think the authors need to de more explicit about what the slab model is.

Response: The ocean temperature in the slab model is diagnosed from the heat flux exchange among the atmosphere, ocean and ice model, without the ocean dynamics process. The ocean temperature is also output from the ice model, together with the surface ocean currents. However, we are not sure whether the surface ocean currents are involved during the model integration so far. Thus, results from the slab ocean model are no longer analyzed in our revised manuscript.

14. Line 355: Seems like the authors have the means to provide a further explanation, why not figure this out an include it in this paper?

Response: As our response to comment #13, results from the slab ocean model are no longer presented in our revised manuscript.

Reference:

Dinniman, M. S., and Rienecker, M. M.: Frontogenesis in the North Pacific oceanic frontal zones: a numerical simulation, J. Phys. Oceanogr., 29(4), 537-559, doi: 10.1175/1520-0485(1999)029<0537:FITNPO>2.0.CO;2, 1999.

Kazmin, A. S., and Rienecker, M. M.: Variability and frontogenesis in the large-scale oceanic frontal zones, J. Geophys. Res., 101(C1), 907-921, doi: 10.1029/95JC02992, 1996.

Qiu, B., and Chen Q. M.: Eddy-induced heat transport in the subtropical North Pacific from Agro, TMI, and Altimetry Measurements. J. Phys. Oceanogr., 35, 458-473, doi: 10.1175/JPO2696.1, 2005.

Qiu, C. H., and Kawamura, H: Study on SST front disappearance in the subtropical North Pacific using microwave SSTs. J. Oceanogr., 68, 417-426, doi: 10.1007/s10872-012-0106-z, 2012.

Wunsch, C.: Where do ocean eddy heat fluxes matters? J. Geophys. Res., 104, 13235-13249, doi: 10.1029/1999JC900062, 1999.

Responses to Reviewer #2

We appreciate the reviewer's comments and suggestions on our manuscript. Our replies follow each of Reviewer's comments or suggestions. The revised text in our revised manuscript is highlighted in red.

Comments:

1. Line 51: "respective"-> "perspective"

Response: Revised.

2. Line 187-188: Authors should give some explanations about how "the residual term (R) is mainly positive and facilitates an increasing SST" and how "the residual term acts to suppress SST decreasing tendency (Line 197)", since term R represents sub-scale process and dissipation.

Response: The residual term beneficial to an increasing SST may be associated with the meridional eddy heat fluxes over the subtropical North Pacific. Wunsch (1999) noted that eddy-induced heat fluxes are important relative to the total meridional heat fluxes in western boundary current regions of the North Atlantic and Pacific Oceans. Moreover, Qiu and Chen (2005) showed that the meridional eddy-induced heat fluxes

over the subtropical North Pacific are both poleward for warm-core eddy detected in 11 Mar–3 Jun 2001 and cold-core eddy detected in 30 Dec 2001–24 Feb 2002. Accordingly, the poleward eddy-induced heat fluxes tend to transport the warm water from lower latitude to the subtropics, and benefit the warmer water there. These findings are consistent with our results that the residual term leads to the increasing SST over the NPSTF. Thus, the residual term beneficial to an increasing SST over the NPSTF is very likely due to the meridional eddy fluxes. However, it is still hard to confirm this process at this stage due to the relatively coarse resolutions of the data used in study. Thus, further exploration is needed when finer data becomes available to us. We add this discussion in our revised manuscript (see lines 366-380 on page 19).

3. Line 203-204: Authors can not consider that "the GM tendency is mainly caused by the net heat flux term (Fig. 5e)". For example, at 26.5°N, GM tendency increases temporally from October to the middle of December, however, the net heat flux term experiences a decreasing period from October to the end of December. In fact, vadv term and R term also contribute to GM tendency especially in January and February.

Response: Although the magnitude of the net heat flux dominates the GM tendency from October to December, the tendency of GM tendency is not consistent with that of the net heat flux term at 26.5°N. However, the increasing of the GM tendency corresponds to that of meridional temperature advection, highlighting the important role of the meridional temperature advection in the frontogenesis. We add this discussion in our manuscript (see lines 246-251 on page 13).

4. Authors should not cap the GM tendency at 100% in October and November in Fig. 6b.

Response: Revised.

5. Fig.7 could be omitted.

Response: The results from Argo data in Figure 7 is shown to confirm the conclusion that both the net heat flux and the meridional temperature advection are beneficial to the NPSTF frontogenesis from SODA. However, we also found that the meridional temperature advection in Argo data dominates the frontogenesis in January and February, highlighting the importance of the meridional temperature advection. Thus, results from SODA and Argo data exhibit some small differences. So we prefer to show this figure and move it into Figure 6.

6. Caption of Figure 8: It is the contribution of individual radiation component to the GM tendency.

Response: Fixed.

7. Line 269-270: How to estimate a 75% contribution of Ekman convergence to the meridional temperature in January and February.

Response: We separate the contribution of the Ekman convergence to the meridional temperature advection into the contribution of individual positive and negative values, because only positive values of the meridional temperature advection and Ekman convergence benefit the frontogenesis of the NPSTF. The contributions of positive values, regionally-averaged over 140°–190°E, 24°–28°N, are 78% and 84% in January and February, respectively. As for the negative values (i.e., suppressing the frontogenesis), the Ekman convergence is much smaller than the meridional temperature advection. Thus, we consider that the Ekman convergence accounts for at least 75% of the meridional temperature advection in January and February in terms of the contribution to the frontogenesis. However, this conclusion seems to be inadequate. Thus, this statement is revised as: “In terms of magnitude, the Ekman convergence also largely contributes to the meridional temperature advection in the frontogenesis.”(see lines 280-281 on page 15)

8. Line 334-338: “The thermodynamic calculation uses a specified mixed-layer depth, and the temperature of the slab is calculated based on the mixed-layer depth

and surface fluxes. It means that the ocean dynamics processes can be ignored and the SST variation responds to the atmosphere." Why? Since "The SST and meridional oceanic current velocity from the last 15 model years are used for analyses. (Line 342-343)" and "suggesting ocean dynamics may play an important role in the northward migration process (Line 354-355)".

Response: The SST diagnosed in the slab ocean model is related to the surface heat fluxes among the atmosphere, ocean and ice model, without any oceanic internal dynamics process. Thus, the SST in the slab ocean model is considered irrelevant with the ocean process. As suggested in comment#9, results from the slab ocean model are no longer analyzed in our revised manuscript.

9. Section 4.3 about analysis with model outputs is unnecessary since no additional sensitivity experiment was carried out, the model output itself only provide misrepresented "observations".

Response: As suggested, results from the slab ocean model are no longer analyzed in our revised manuscript.

10. Check the caption of Figure 13.

Response: Fixed.

Reference:

Qiu, B., and Chen Q. M.: Eddy-induced heat transport in the subtropical North Pacific from Agro, TMI, and Altimetry Measurements. J. Phys. Oceanogr., 35, 458-473, doi: 10.1175/JPO2696.1, 2005.

Wunsch, C.: Where do ocean eddy heat fluxes matters? J. Geophys. Res., 104, 13235-13249, doi: 10.1029/1999JC900062, 1999.

List of changes in the manuscripts：

1. **Lines 16-19 on page 2:** clarify the new findings in this manuscripts (response to the reviewer1's point 11)
2. **Line 54 on page 4:** revised the "perspective" (response to the reviewer2's point 1)
3. **Lines 62, 84, 95, 108 and 110:** revised the "heat budget equation" (response to the reviewer1's point 2)
4. **Lines 102 on page 7:** clarify the interpolated data (response to the reviewer1's point 1)
5. **Line 104 on page 7:** clarify the atmospheric data used in this study (response to the reviewer1's point 1)
6. **Lines 150-152 on page 9:** clarify the "maximum center expanding" (response to the reviewer1's point 6)
7. **Line 156 on page 9:** corrected the "except" (response to the reviewer1's point 8)
8. **Lines 163-165 on page 9:** add the discussion about the zonal velocity surprisingly weak in the region of strongest SST gradient (response to the reviewer1's point 7)
9. **Lines 246-251 on page 13:** add the discussion about the GM tendency is not consistent with that of the net heat flux at 26.5°N (response to the reviewer2's point 3)
10. **Lines 280-281 on page 15:** revised the statement (response to the reviewer2's point 7)
11. **Delete the Section4.3** according to the reviewer2's point 9
12. **Lines 336-343 on page 18:** clarify the new findings in this manuscripts (response to the reviewer1's point 11)
13. **Lines 366-380 on page 19:** add the discussion about the residual term in our study (response to the reviewer1's points 3 and 10 and reviewer2's point 2)
14. **Lines 535-540 on page 27:** add the definition of winter and spring time period and show the key area of NPSTF (response to the reviewer1's points 4 and 5)
15. **Lines 570-577 on page 32:** revised the Figure 6b and move the Figure 7 to the Figure 6c (response to the reviewer2's points 4 and 5)
16. **Lines 582-586 on page 33:** revised the caption of Figure 8 (response to the

reviewer2’s point 6)

17. **Delete the Figure 10** according to the reviewer1’s point 12
18. **Delete the Figure 13** according to the reviewer2’s point

North Pacific subtropical sea surface temperature frontogenesis and its connection with the atmosphere above

Leying Zhang[1,2], Haiming Xu[1], Jing Ma[1], Ning Shi[1], Jiechun Deng[1,3]

1. *Collaborative Innovation Center on Forecast and Evaluation of Meteorological Disasters (CIC-FEMD) / Key Laboratory of Meteorological Disaster, Ministry of Education (KLME) /Joint International Research Laboratory of Climate and Environment Change (ILCEC), Nanjing University of Information Science & Technology, Nanjing 210044, China*
2. *Joint Innovation Center for Modern Forestry Studies, College of Biology and Environment, Nanjing Forestry University, Nanjing 210037,China*
3. *Department of Atmospheric and Environmental Science, University at Albany, State University of New York, Albany, NY 12222, USA*

ABSTRACT

The net heat flux and meridional temperature advection in the ocean are two factors in the North Pacific subtropical sea surface temperature front (NPSTF) frontogenesis occurring from October to the following February. However, relative importance of these two factors has been rarely explored. In this study, frontogenesis of the NPSTF is examined quantitatively based on the mixed-layer heat budget equation to clarify the relative importance of net heat flux and meridional temperature advection, and to further explore its connection with the atmosphere above. Diagnosis results show that the net heat flux dominates the frontogenesis from October to December, while the meridional temperature advection in the ocean contributes equally as or even more than the net heat flux in January and February. The atmosphere is critical to the frontogenesis of the NPSTF, including the direct effect of the net heat flux and the indirect effect through the Aleutian low. Further analyses demonstrate that the latent heat flux (the shortwave radiation) dominates the net heat flux in October (from November to February). The meridional temperature advection in the ocean is mostly owing to the meridional Ekman convergence, which is related to the Aleutian low. Climatologically, the strengthening and southward migration of the Aleutian low from October to the following February are characterized by the acceleration and southward shift of the westerly wind to the south, respectively, which can drive southward ocean currents. Correspondingly, the southward ocean currents give the colder meridional advection to the north of the NPSTF in January and February, favoring the frontogenesis. In addition, the Aleutian low plays a role in

transforming the dominant effect of the net heat flux to the joint effect of the meridional temperature advection and the net heat flux in January.

Key words: North Pacific subtropical sea surface temperature front; frontogenesis; net heat flux; meridional temperature advection; Aleutian low

1. Introduction

The North Pacific Ocean is featured by two zonal sea surface temperature (SST) fronts at mid-latitude and subtropics, respectively. The mid-latitude front, with greater magnitude, is referred to as the North Pacific subarctic SST front (NPSAF), and the subtropical one is the North Pacific subtropical SST front (NPSTF). Due to the smaller magnitude, the NPSTF has been rarely studied. However, it also exerts significant influences on the overlying atmosphere (Xie, 2004; Kobashi et al., 2008; Wang et al., 2016; Zhang et al., 2017a, 2017b). On the synoptic scale, Kobashi et al. (2008) found that the subsynoptic lows along the NPSTF are enhanced by the condensational heating and baroclinicity associated with the NPSTF during April to May. On the interannual scale, the intensified NPSTF in spring can not only accelerate the East Asian westerly jet (Zhang et al., 2017a), but also serve as a precursor to the following La Niña event (Zhang et al., 2017b).

From the perspective of the seasonal variation, the NPSAF can exist throughout the year, but the NPSTF is robust in winter and spring and is absent in summer and autumn (Fig. 1; Kobashi and Xie, 2012). Thus, several studies have focused on the frontogenesis and frontolysis of the NPSTF (Roden, 1975; Kazmin and Rienecker, 1996; Qiu and Kawamura, 2012). It is pointed out that the net heat flux is responsible for the frontolysis of the NPSTF (Qiu and Kawamura, 2012; Qiu et al., 2014). In terms of the frontogenesis, Roden (1975) found the meridional Ekman convergence is the primary reason for the frontogenesis of the NPSTF. However, Kazmin and Rienecker (1996) diagnosed the mixed-layer heat budget equation using the

observation data from 1982 to 1990, and pointed out that both the net heat flux and the Ekman convergence are frontogenetic and equally important to provide the observed frontogenesis in winter, rather than the Ekman convergence alone. This finding is further confirmed by Dinniman and Rienecker (1999), based on the 10 years' (1985-1995) simulation of a primitive equation model (Geophysical Fluid Dynamics Laboratory's MOM2). However, they argued that these two factors are not equally important: the net heat flux (the Ekman convergence) dominates the frontogenesis in the western subtropical Pacific (the central and eastern subtropical Pacific). Thus, the relative role of the net heat flux and the Ekman convergence in the frontogenesis of the NPSTF remains unclear, due to limited data used in previous studies. Meanwhile, the net heat flux is associated with the air-sea interaction, and the Ekman convergence is driven by the surface wind stress, implying that both frontogenesis factors are closely related to the atmospheric circulation. Kazmin (2017) demonstrated the long-term (quasi-decadal) variability of the subtropical SST front is determined by the variability of the meridional shear of the zonal wind. Thus, the role of the atmosphere in the frontogenesis of the NPSTF deserves to further study.

Therefore, this paper aims to figure out the relative importance of the net heat flux and the oceanic meridional temperature advection (including the Ekman convergence) in the frontogenesis of the NPSTF, especially the role of the atmosphere in this process. The rest of the paper is organized as follows. We introduce the data and methods in Section 2. We analyze the frontogenesis of the NPSTF using the mixed-layer heat budget equation in Section 3 to explore the relative importance of

the net heat flux and the oceanic meridional temperature advection. Section 4 further investigates the roles of atmosphere in the frontogenesis. Conclusion and discussion are given in Section 5.

2 Data and Methods

2.1 Data

We use the monthly ocean temperature, current velocities and wind stress from the Simple Ocean Data Assimilation (SODA; Carton and Giese, 2008) version 2.2.4 at 0.5°×0.5° grid with 40 levels from the depth of 5 to 2000 m. We also use surface heat fluxes from the Objectively Analyzed Air-sea Fluxes Project (OAFlux; Yu and Weller, 2007) at 2.5°×2.5° grid to examine the mixed-layer heat budget. All heat fluxes are defined to be positive downward. For consistency, all variables are interpolated onto 0.5°×0.5° grid, and they cover the period from January 1984 to December 2009. The ocean temperature at 1.0°×1.0° grid with 27 levels from the International Pacific Research Center (IPRC) Argo Product, together with ocean currents (on 40 levels) and surface heat fluxes at 0.3°×1.0° grid from the NCEP Global Ocean Data Assimilation System (GODAS; Saha et al., 2011) are used to confirm our results based on the SODA data. The Argo and GODAS data are interpolated onto 1.0°×1.0° grid at 27 depths, and only cover the period from January 2005 to December 2013.

The atmospheric geopotential height and winds used in this study are monthly ERA-interim reanalysis from the European Center for Medium-range Weather Forecasts (ECMWF; Dee et al., 2011). They are on 1.5°×1.5° grid, and cover the

period from January 1984 to December 2009.

2.2 The mixed-layer heat budget equation

The temporal variation of SST is governed by mixed-layer dynamics, which can be represented by the mixed-layer heat budget equation (Dinniman and Rienecker, 1999; Zhang et al., 2013):

$$\frac{\partial SST}{\partial t} = -u\frac{\partial SST}{\partial x} - v\frac{\partial SST}{\partial y} - w\frac{\Delta T}{H} + \frac{Q_{net}}{\rho_0 c_p H} + R, \quad (1)$$

where SST denotes sea surface temperature (here, we assume that SST equals mixed-layer mean temperature), and ΔT represents the temperature difference between the mixed layer and the interior ocean immediately below the mixed layer. u and v are mixed-layer zonal and meridional oceanic current velocities, respectively; w is the vertical velocity at the bottom of the mixed layer. H is mixed-layer depth. Q_{net} is the net surface heat flux, including sensible and latent heat fluxes, as well as longwave and shortwave radiation. A positive value of Q_{net} means that the ocean gains heat from the atmosphere. ρ_0 and c_p are the density and heat capacity of sea water, respectively. R is the residual term, including sub-grid scale processes and dissipation. The zonal temperature advection ($-u\partial SST/\partial y$), meridional temperature advection ($-v\partial SST/\partial y$) and vertical temperature advection ($-w\Delta T/H$) are intrinsic processes in the ocean (Yu and Boer, 2004; Chen et al., 2014), while the net heat flux term ($Q_{net}/\rho_0 c_p H$) represents air-sea interaction. The SST tendency ($\partial SST/\partial t$) in a particular month is obtained through the central finite difference.

Since the meridional gradient of SST overwhelmingly dominates over its zonal

128 counterpart in the frontal region, the gradient magnitude (GM) of the NPSTF is
129 defined as $GM = -\partial SST/\partial y$ to measure the intensity of the NPSTF in a particular
130 month (Qiu and Kawamura, 2012; Qiu et al., 2014). Accordingly, GM is always
131 positive because the climatological mean SST is higher in the south. Its tendency can
132 be derived from Eq. (1) as follows,

133 $$\frac{\partial GM}{\partial t} = \frac{\partial}{\partial y}\left(u\frac{\partial SST}{\partial x}\right) + \frac{\partial}{\partial y}\left(v\frac{\partial SST}{\partial y}\right) + \frac{\partial}{\partial y}\left(w\frac{\Delta T}{H}\right) - \frac{\partial}{\partial y}\left(\frac{Q_{net}}{\rho_0 c_p H}\right) - \frac{\partial R}{\partial y}, \quad (2)$$

134 A bigger (smaller) GM indicates a stronger (weaker) NPSTF. A positive GM tendency
135 ($\partial GM/\partial t$) suggests a process that GM gradually increases, corresponding to the
136 frontogenesis of the NPSTF. A negative GM tendency indicates the decreasing of GM,
137 corresponding to the frontolysis of the NPSTF.

138 2.3 Definition of the mixed-layer depth

139 Three definitions of mixed-layer depth H are used in this study: (a)
140 $SST - T_H = 0.5°C$ (Qiu et al., 2014), where T_H is the temperature at the base of
141 the mixed layer, and the depth of 0.5°C lower than the SST is defined as H. (b)
142 $SST - T_H = 1.0°C$ (Suga and Hanawa, 1990), so the depth of 1.0°C lower than
143 the SST is defined as H. (c) mixed-layer depth from the GODAS. Figure 2a shows the
144 latitude-time section of the climatological mean mixed-layer depth calculated by
145 method (a) averaged from 140°E to 170°W (longitudinal region of the NPSTF in Fig.
146 1; Zhang et al., 2017). The mixed-layer depth exhibits significant seasonal variation,
147 namely, deep in winter and spring with a maximum of 60–80 m and shallow in
148 summer with a minimum of 20 m. Figure 2b shows the latitude-depth section of the

149 climatological mean zonal current velocities and ocean temperature gradients
150 averaged in winter and spring when the NPSTF exists. The maximum center of the
151 ocean temperature gradients (NPSTF) is mainly located between 24°N and 30°N at
152 surface and could expand downward to the depth of 60 m. The vertical scale of the
153 maximum center is consistent with the deeper mixed layer in winter and spring
154 calculated by method (a), suggesting the variation of mixed-layer-averaged
155 temperature gradient can well represent the variation of the NPSTF. The mixed-layer
156 depth is also computed by methods (b) and (c). Except for the deeper depth in winter
157 and spring (~80 m), their temporal evolutions of the mixed-layer depth agree well
158 with that in Fig. 2a, and the diagnosis results of Eqs. (1) and (2) do not change
159 qualitatively (not shown). Therefore, method (a) is used to define the mixed-layer
160 depth in this study. In addition, two subsurface subtropical temperature fronts are
161 located between 80 and 180 m in Fig. 2b, associated with the two branches of the
162 North Pacific subtropical countercurrent, consistent with the findings of Kobashi et al.
163 (2006). Note that the eastward velocities are relatively weak over 25°N–30°N where
164 the ocean temperature gradients are strongest. This may be due to the offset of the
165 salinity gradients, which yield westward zonal velocities there (not shown).
166
167 **3 Frontogenesis of the NPSTF**
168 Figure 3 shows latitude-time sections of the climatological mean GM and its
169 tendency averaged over (140°E–170°W). The GM tendency is positive and moves
170 southward from September to the following February. The NPSTF that forms in

December is characterized by the SST gradient of 0.6 °C (100 km)$^{-1}$, which is the threshold for the emergence and disappearance of the NPSTF according to Qiu et al. (2014). Then, it strengthens and slightly migrates southward until March, with a maximum of 0.9 °C (100 km)$^{-1}$ at 27°N. Although the NPSTF is still robust in spring, it exhibits an evident northward shift with a strengthening in the northern part and a weakening in the southern and central parts. It finally disappears in July, consistent with the previous studies (Dinniman and Rienecker, 1999; Qiu et al., 2014). In this study, we mainly focus on the frontogenesis period of the NPSTF, which is from October to the following February when the GM tendency is significantly positive. As the NPSTF is located between 24°N and 30°N during this period, the frontogenesis region of the NPSTF is defined as (140°E–170°W, 24°N–30°N).

3.1 SST variation

Since the NPSTF is characterized by the meridional gradient of SST in the subtropics, the SST variation during the frontogenesis of the NPSTF is the first thing we are interested in. Figure 4 portrays the temporal evolution of each term in Eq. (1) over the NPSTF from October to the following February. As shown in Fig. 4a, the SST tendency is coherently negative during the frontogenesis, indicating that the SST across the NPSTF gradually decreases. Note that the SST decreases more quickly in the north than in the south, corresponding to the strengthening of the NPSTF. This indicates that the largely decreasing SST in the north should be the key for the frontogenesis of the NPSTF. A diagnosis of each contributor on the right-hand side of Eq. (1) is given in Figs. 4b–f. The SST tendency due to the net heat flux term (Fig. 4e)

bears similarities with the SST tendency in Fig. 4a in terms of spatial pattern and magnitude, while the residual term (R) is mainly positive and facilitates an increasing SST. As for the oceanic intrinsic processes, the meridional temperature advection serves as a much more important factor in determining the SST tendency compared to the zonal and vertical temperature advections, especially in January and February. In addition, the meridional temperature advection experiences a significant southward displacement, which slightly increases the SST across the NPSTF in October and November and strongly decreases the SST in January and February. This is similar to the southward migration of the GM tendency during the frontogenesis (Fig. 3). Overall, the SST across the NPSTF gradually decreases during the frontogenesis, which is mainly attributed to the net heat flux term with some contributions from the cold meridional advection in January and February. The residual term acts to suppress this decreasing tendency.

3.2 GM variation

Figure 5a shows the temporal evolution of the climatological mean GM tendency across the NPSTF from October to the following February. It is positive and moves southward during the frontogenesis period, corresponding to the gradual enhancement of the NPSTF. Similar to the SST tendency from October to December (Fig. 4), the GM tendency is mainly caused by the net heat flux term (Fig. 5e), while the residual term acts to suppress the frontogenesis process (Fig. 5f). In January and February, the net heat flux term, together with the meridional temperature advection, favors the frontogenesis of the southern and central NPSTF and suppresses the frontogenesis of

215 the northern NPSTF. The effect of *R* is nearly the opposite. Note that the magnitude of
216 the meridional temperature advection is quantitatively comparable to that of the net
217 heat flux term in January and February. Besides, the zonal and vertical temperature
218 advections are negligible due to their smaller magnitudes (Figs. 5b and 5d). Figure 6a
219 further shows the regionally averaged GM tendency across the NPSTF during the
220 frontogenesis. The net heat flux term dominates the GM tendency from October to
221 December and decreases after January. The meridional temperature advection
222 increases gradually from October to December, and plays an important role in January
223 and February. The residual term (*R*) mainly exerts an opposing influence on the
224 frontogenesis except in January. These findings can be quantitatively illustrated in Fig.
225 6b. The net heat flux term controls the NPSTF frontogenesis from October to
226 December, while the meridional advection increases gradually and contributes equally
227 as the net heat flux in January and February. The results in January and February are
228 consistent with those in Kazmin and Rienecker (1996), namely, the net heat flux and
229 the meridional Ekman convergence are equally important for the frontogenesis in
230 winter. In addition, the net heat flux also contributes to the disappearance of the
231 NPSTF in summer (not shown), which is consistent with the finding of Qiu et al.
232 (2014).

233 Figure 6c shows the area mean GM tendency across the NPSTF calculated using
234 the Argo data from 2005 to 2013. Similar to Fig. 6a, the net heat flux term dominates
235 from October to December and the meridional temperature advection works in
236 January and February. However, the effect of the meridional temperature advection is

overwhelmingly large in January and February, with much smaller net heat flux term and *R*. This further confirms the dominant effect of the net heat flux term from October to December and the important role of the meridional temperature advection in January and February for the frontogenesis of the NPSTF. Therefore, similar to the previous studies (Kazmin and Rienecker, 1996; Dinniman and Rienecker, 1999), both the net heat flux and oceanic meridional temperature advection contribute to the frontogenesis of the NPSTF. As for the relative importance, the net heat flux dominates the frontogenesis from October to December and then the meridional temperature advection contributes equally as or even more than the net heat flux in January and February. In addition, although the magnitude of the net heat flux dominates the GM tendency from October to December, the tendency of GM tendency is not all consistent with that of the net heat flux term, for example at 26.5°N (Fig. 5e). However, the increasing of the GM tendency corresponds to that of meridional temperature advection, highlighting the important role of the meridional temperature advection in the frontogenesis.

4 Roles of the Atmosphere

4.1 Decomposition of the net heat flux

The net heat flux term is critical for the frontogenesis of the NPSTF from October to December, which can be decomposed as follows:

$$\frac{Q_{net}}{\rho_0 c_p H} = \frac{Q_S}{\rho_0 c_p H} + \frac{Q_L}{\rho_0 c_p H} + \frac{Q_{LR}}{\rho_0 c_p H} + \frac{Q_{SR}}{\rho_0 c_p H}, \quad (3)$$

where Q_S, Q_L, Q_{LR}, and Q_{SR} represent sensible heat flux, latent heat flux, longwave radiation, and shortwave radiation, respectively. Figure 7 shows the temporal evolution of the GM tendency induced by individual heat flux terms in Eq. (3). The positive latent heat flux term primarily contributes to the positive GM tendency in October, together with the sensible heat flux and the longwave radiation terms. The shortwave radiation term evidently strengthens in November and December, and appears to be the dominant factor in January and February. Meanwhile, the other three terms act to suppress the frontogenesis, especially the latent heat flux term. Therefore, the four components of the net heat flux jointly contribute to the frontogenesis of the NPSTF, with a leading effect of the latent heat flux term in October and shortwave radiation term from November to February. Note that the temporal variation of the net heat flux term is consistent with that of the latent heat flux term. Moreover, the quick decrease of the net heat flux term in January is mainly attributed to the reduction of the latent heat flux term.

4.2 Cold meridional advection

As discussed above, the meridional temperature advection plays an important role in the frontogenesis of the NPSTF in January and February (Fig. 6), which transports the cold water from north to decrease the SST across the NPSTF. Figure 8 gives the meridional Ekman convergence of $\partial(V_E \partial SST/\partial y)/\partial y$ calculated by the meridional Ekman velocity $V_E = -\tau_x/\rho_0 fH$, where τ_x is the zonal component of wind stress and f is the Coriolis parameter. The meridional Ekman convergence moves southward from October and strengthens in January and February, similar to the meridional

temperature advection (Fig. 5c). In terms of magnitude, the Ekman convergence also largely contributes to the meridional temperature advection in the frontogenesis. Thus, the meridional temperature advection in January and February is mostly owing to the meridional Ekman convergence. Note that $\tau_x = c_D \rho_a U^2$, where c_D is the drag coefficient, ρ_a is air density and U is the surface zonal wind speed. Accordingly, the meridional Ekman convergence must be associated with zonal wind speed. In the following, we focus on possible atmospheric influence on the meridional temperature advection.

Figure 9a shows latitude-time sections of the climatological monthly mean geopotential height and zonal wind speed at 1000 hPa. The Aleutian low strengthens and heads southward from ~48°N in October to ~35°N in February, with the associated westerly wind enhanced and shifted southward. In theory, the westerly wind stress co-varies with the westerly wind, which can force southward Ekman ocean currents in the Northern Hemisphere according to $V_E = -\tau_x / \rho_0 fH$. Thus, the southward meridional ocean currents are obviously increased, and move southward from October to the following February with the Aleutian low (Figure 9b). Correspondingly, the cold meridional advection is enhanced and moves southward, cooling the SST across the NPSTF in January and February, which is consistent with the southward migration of the meridional temperature advection in Fig. 4c. Li (2010) found that an Aleutian low-like anomalous wind stress can decrease the SST in the mid-latitude North Pacific (north of 25°N) in numerical models. Further analysis revealed that it is the cold meridional advection, induced by the Aleutian low-like

anomalous wind stress, acts to decrease the SST north of 25°N. This previous study suggested that the strengthening and southward migration of the Aleutian low can decrease the SST across the NPSTF via the cold meridional advection. In addition, both the westerlies and the southward currents reach the southern latitude of 28°N, resulting in colder SST in the northern NPSTF than in the southern NPSTF, corresponding to the frontogenesis of the NPSTF. The cooler SST in the northern is also associated with the fact that the northern SST cooling contributes greatly during the frontogenesis (Fig. 4a). Thus, the meridional Ekman convergence dominates the cold meridional advection, which may be related to the strengthening and southward migration of the Aleutian low from October to the following February. The associated westerly wind, together with the wind-driven southward currents, is strengthened and shifts southward to induce cooler SST in the northern NPSTF, favoring its frontogenesis.

Note that the rapid decrease of the net heat flux term in January is mainly due to the reduction of the latent heat flux term. The latent heat flux term can be calculated by $Q_L = \rho_a L C_E U_{10m}(q_s - q_a)$, where L is the latent heat of vaporization, C_E is the bulk coefficient, U_{10m} represents the 10-m wind speed (Qiu et al., 2014). According to Eq. (2), the GM tendency is proportional to the meridional gradient of the 10-m wind speed ($-\partial U_{10m}/\partial y$). Figure 10 shows the temporal evolutions of $-\partial U_{10m}/\partial y$ across the NPSTF and GM tendency associated with the latent heat flux term. The meridional gradient of wind speed gradually decreases from October to the following February, consistent with the GM tendency calculated by the latent heat flux term,

especially from December to February. Interestingly, the decreasing $-\partial U_{10m}/\partial y$ is also consistent with the southward migration of the Aleutian low (blue line in Fig. 10). This southward shift leads to a gradual increase in the wind speed to the south of the Aleutian low (to the north of the NPSTF), corresponding to the decrease of $-\partial U_{10m}/\partial y$ between the NPSTF and its northern region, further resulting in the decease of the latent heat flux term during the frontogenesis. Therefore, the Aleutian low acts to decrease the effect of the net heat flux and to increase the effect of the meridional temperature advection during the frontogenesis, which may also play an important role in transforming the dominant effect of the net heat flux to the joint effect of the meridional temperature advection and net heat flux in January.

5. Conclusion and discussion

Previous studies have demonstrated that both net heat flux and meridional temperature advection in the ocean contribute to the NPSTF frontogenesis (Kazmin and Rienecker, 1996; Dinniman and Rienecker, 1999). However, relative importance of these two factors in the frontogenesis is not stated clearly. In this study, we investigated the frontogenesis of the NPSTF occurring from October to the following February based on the mixed-layer heat budget equation, and further find that the net heat flux and meridional temperature advection play different roles in the different periods of the frontogenesis. The net heat flux dominates the frontogenesis of the NPSTF from October to December, while the meridional temperature advection contributes equally as or even more than the net heat flux in January and February.

346 The zonal and vertical temperature advections can be neglected due to their smaller
347 magnitudes, while *R* acts to suppress the frontogenesis except in January.

348 Moreover, the role of the atmosphere in the frontogenesis is also explored,
349 including the direct effect of the net heat flux and the indirect effect through the
350 Aleutian low. A decomposition of the net heat flux term reveals that its four
351 components jointly contribute to the frontogenesis, with a leading role by the latent
352 heat flux in October and by shortwave radiation from November to the following
353 February. Further analyses of atmospheric effects on the oceanic process show that the
354 meridional Ekman convergence dominates the meridional temperature advection, and
355 is associated with the Aleutian low variation. The strengthening and southward
356 migration of the Aleutian low are characterized by the acceleration and southward
357 shift of the westerly wind to the south, which benefits southward ocean currents.
358 Accordingly, the cold meridional advection due to the southward currents induces
359 cooler SST in the northern NPSTF than in the southern NPSTF, and favors the
360 frontogenesis of the NPSTF in January and February. In addition, the reduction of the
361 latent heat flux term (dominating the net heat flux term variation) during the
362 frontogenesis also results from the southward shift of the Aleutian low, suggesting
363 that the Aleutian low also plays a role in transforming the dominant effect of the net
364 heat flux to the joint contributions of meridional temperature advection and the net
365 heat flux in January.

366 Note that the residual term, including the sub-grid scale process, is relatively large
367 in our results, which may be due to the eddy-induced heat fluxes. Wunsch (1999)

noted that eddy-induced heat fluxes are important relative to the total meridional heat fluxes in western boundary current regions of the North Atlantic and Pacific Oceans. Moreover, Qiu and Chen (2005) showed that the meridional eddy-induced heat fluxes over the subtropical North Pacific are both poleward for warm-core and cold-core eddies. Accordingly, the poleward eddy-induced heat fluxes tend to transport the warm water from lower latitude to the subtropics, and benefit the warmer water there. These findings are consistent with our result that the residual term leads to the increasing SST over the NPSTF. Thus, the eddy-induced heat flux may play an important role in the residual term to increase the SST and to further halt the frontogenesis (Figs. 4f and 5f). However, it is still hard to confirm this process at this stage because the spatial and temporal resolutions of observation and reanalysis data used in study are relatively coarse. Thus, further exploration is needed when finer data becomes available to us.

Data availability. The SODA, Argo and GODAS data can be downloaded fro m: http://apdrc.soest.hawaii.edu/data/data.php. The OAFlux data are from: ftp://ft p.whoi.edu/pub/science/oaflux/data_v3/monthly/radiation_1983-2009/, and the ER A-interim data are form: http://apps.ecmwf.int/datasets/data/interim-full-moda/levt ype=sfc/.

Competing Interests. The authors declare that they have no conflict of interes t.

Acknowledgements. This work was jointly supported by the National Science Foundation of China (Grant Nos. 41575077, 41490643, 41575057, 41705054 and 41805051) and the National Key Research and Development Program of China (2017YFA0604102). L Zhang was supported by the scientific research start-up funds of Nanjing Forestry University (Grant No.163108056). J Deng was supported by the General Program of Natural Science Research of Jiangsu Province University (Grant No.17KJB170012) and the China Scholarship Council (Grant No.201808320137).

References

Carton, J. A., and Giese, B. S.: A reanalysis of Ocean Climate Using Simple Ocean Data Assimilation, Mon. Weath. Rev., 136(8), 2999-3017, doi: 10.1175/2007MWR1978.1, 2008.

Chen, S. F., Yu, B., and Chen, W.: An analysis on the physical process of the influence of AO on ENSO, Clim. Dyn., 42(3-4), 973-989, doi: 10.1007/s00382-012-1654-z, 2014.

Dee, D. P., Uppala, S. M., and Simmons, A. J.: The ERA-interim reanalysis: configuration and performance of the data assimilation system, Quarterly Journal of the Royal Meteorological Society, 137(656), 553-597, doi:10.1002/qj.828, 2011.

Deng, J. C., Xu, H. M., Shi, N., Zhang, L. Y., and Ma, J.: Impacts of northern Tibetan Plateau on East Asian summer rainfall via modulating midlatitude transient eddies, J. Geophys. Res. Atmos., 122, 8667-8685, doi: 10.1002/2017JD027034, 2017.

412 Dinniman, M. S., and Rienecker, M. M.: Frontogenesis in the North Pacific oceanic
413 frontal zones: a numerical simulation, J. Phys. Oceanogr., 29(4), 537-559, doi:
414 10.1175/1520-0485(1999)029<0537:FITNPO>2.0.CO;2, 1999.
415 Kazmin, A. S.: Variability of the climatic oceanic frontal zones and its connection
416 with the large-scale atmospheric forcing, Process in Oceanography, 154, 38-48,
417 doi: 10.1016/j.pocean.2017.04.012, 2017.
418 Kazmin, A. S., and Rienecker, M. M.: Variability and frontogenesis in the large-scale
419 oceanic frontal zones, J. Geophys. Res., 101(C1), 907-921, doi:
420 10.1029/95JC02992, 1996.
421 Kiehl, J. T., Shields, C. A., Hack, J. J., and Collins, W. D.: The climate sensitivity of
422 the community climate system model version 3 (CCSM), J. Clim., 19, 2584-2596.
423 doi: 10.1175/JCLI3747.1, 2006.
424 Kobashi, F., Mitsudera, H., and Xie, S. P.: Three subtropical fronts in the North
425 Pacific: Observation evidence for mode water-induced subsurface frontogenesis, J.
426 Geophys. Res.:Oceans, 111(9), 616-627, doi: 10.1029/2006JC003479,2006, 2006.
427 Kobashi, F., and Xie, S. P.: Interannual variability of the North Pacific subtropical
428 countercurrent: Role of local ocean-atmosphere interaction, J. Oceanogr., 68,
429 113-126, doi: 10.1007/s10872-011-0048.x, 2012.
430 Kobashi, F., Xie, S. P., Iwasaka, N., and Sakamoto T. T.: Deep atmospheric response
431 to the North Pacific oceanic subtropical front in spring, J. clim., 21, 5960-5975,
432 doi: 10.1175/2008JCLI2311.1, 2008.
433 Li, C.: Variation of wind-driven oceanic gyre in the North Pacific and its feedback to

atmospheric circulation, Qingdao: Ocean University of China. (in chinese), 2010.

Qiu, B., and Chen Q. M.: Eddy-induced heat transport in the subtropical North Pacific from Agro, TMI, and Altimetry Measurements. J. Phys. Oceanogr., 35, 458-473, doi: 10.1175/JPO2696.1, 2005.

Qiu, C., and Kawamura, H.: Study on SST front disappearance in the subtropical North Pacific using microwave SSTs, J. Oceanogr., 68(3), 417-426, doi: 10.1007/s10872-012-0106-z, 2012.

Qiu, C. H., Kawamura, H., Mao, H. B., and Wu, J.: Mechanisms of the disappearance of sea surface temperature fronts in the subtropical North Pacific Ocean, J. Geophys. Res.:Oceans, 119(7), 4389-4398, doi: 10.1002/2014JC010142, 2014.

Roden, G. I.: On North Pacific Temperature, Salinity, Sound Velocity and Density Frontsand their Relation to the Wind and Energy Flux Fields, J. Phys. Oceanogr., 5(4), 557-571, doi: 10.1175/1520-0485(1975)005<0557:ONPTSS>2.0.CO;2, 1975.

Saha, S., Nadiga, S., Thiaw, C., Wang, J., Wang, W., Zhang, Q., van den Dool, H. M., Pan, H. L., Moorthi, S., Behringer, D., Stokes, D., Pena, M., Lord, S., White, G., Ebisuzaki, W., Peng, P., and Xie, P.: The NCEP Climate Forecast System, J. Clim., 19(15), 3483-3517, doi: 10.1175/JCLI3812.1, 2011.

Suga, T., and Hanawa, H.: The mixed-layer climatology in the northwestern part of the north Pacific subtropical gyre and the formation area of subtropical mode water, J. Mar. Res., 48(3), 543-566, doi: 10.1357/002224090784984669, 1990.

Wang, L. Y., Hu, H. B., Yang, X. Q., and Ren, X. J.: Atmospheric eddy anomalies associated with the wintertime North Pacific subtropical front strength and their

457 influence on the seasonal-mean atmosphere, Science Chinese Earth Sciences, 59,
458 2022-2036, doi: 10.1007/s11430-016-5331-7, 2016.
459 Wunsch, C.: Where do ocean eddy heat fluxes matters? J. Geophys. Res., 104,
460 13235-13249, doi: 10.1029/1999JC900062, 1999.
461 Xie, S. P.: Satellite observations of cool ocean-atmosphere interaction, Bull. Am.
462 Meteorol. Soc., 85,195-208, doi: 10.1175/BAMS-85-2-195, 2004.
463 Yu, B., and Boer, G. J.: The role of the western Pacific in decadal variability, Geophys.
464 Res. Lett., 31(2), L02204, doi: 10.1029/2003GL018471, 2004.
465 Yu, L., and Weller, R. A.: Objectively Analyzed air-sea heat Fluxes for the global
466 ice-free oceans (1981–2005), Bull. Ameri. Meteor. Soc., *88*(4), 527-539, doi:
467 10.1175/BAMS-88-4-527, 2007.
468 Zhang, L. Y., Xu, H. M., Shi, N., and Deng, J. C.: Responses of the East Asian Jet
469 Stream to the North Pacific Subtropical Front in spring, Adv. Atmos. Sci., 34(2),
470 144-156, doi: 10.1007/s00376-016-6026-x, 2017a.
471 Zhang, L. Y., Xu, H. M., Shi, N., and Ma, J.: Impact of the North Pacific subtropical
472 sea surface temperature front on El Niño–Southern Oscillation, Int. J. Climatol.,
473 doi: 10.1002/joc.5402, 2017b.
474 Zhang, W. J., Jin, F. F., Zhao, J. X., and Li, J.: On the bias in simulated ENSO SSTA
475 meridional widths of CMIP3 models, J. Clim., 26(10), 3171-3186, doi:
476 10.1175/JCLI-D-12-00347.1, 2013.
477
478

Captions

Figure 1. Climatological meridional SST gradients ($\left|\partial SST/\partial y\right|$, units: °C (100 km)$^{-1}$) in (a) winter, (b) spring, (c) summer, and (d) autumn. The winter refers to the time period of December in preceding year and January-February in the simultaneous year (DJF). The spring, summer and autumn refer to the time period of simultaneous March-Apil-May (MAM), June-July- August (JJA) and September-October- November (SON), respectively. The black boxes in (a) and (b) indicate the key area of the NPSTF.

Figure 2. (a) Latitude-time section of the climatological monthly mean mixed-layer depth (units: m) calculated by $SST - T_H = 0.5°\mathrm{C}$. (b) Latitude-depth section of the climatological zonal current velocity (black contour; units: m s^{-1}), superimposed with ocean temperature gradient (shading; units: °C (100 km)$^{-1}$); both are averaged over winter and spring. All three fields are averaged zonally over (140°E–170°W).

Figure 3. Latitude-time section of the climatological monthly mean gradient magnitude (GM) of the NPSTF (black contour; units: °C (100 km)$^{-1}$) and its tendency (shading; units: °C (100 km)$^{-1}$ month^{-1}), averaged zonally over (140°E–170°W).

Figure 4. Latitude-time section of each term (shading; units: °C month^{-1}) in Eq. (1) from October to the following February, averaged zonally over (140°E–170°W). (a) shows the total SST tendency ($\partial SST/\partial t$), and (b–f) illustrate the components on the right-hand side of Eq. (1), namely, zonal temperature advection (Uadv),

meridional temperature advection (Vadv), vertical temperature advection (Wadv), the net heat flux (Qnet), and the residual term (R). The black contours in each panel are the same, indicating the climatological monthly mean GM (units: °C (100 km)$^{-1}$), averaged zonally over (140°E–170°W).

Figure 5. Same as Fig. 4, except for the terms (units: °C (100 km)$^{-1}$ month^{-1}) in Eq. (2).

Figure 6. (a) The area mean GM tendency (units: °C (100 km)$^{-1}$ month^{-1}) over the NPSTF from October to the following February. (b) The contribution percentages (units: %) of the right-hand side terms in Eq. (2) to the left-hand side term. (c) Same as Fig. 6a, except using the Argo data from 2005 to 2013. The black dashed line in (a) and (c) is the GM tendency of the NPSTF. Green, red, purple, blue, and brown indicate zonal temperature advection (Uadv), meridional temperature advection (Vadv), vertical temperature advection (Wadv), the net heat flux (Qnet), and the residual term (R), respectively.

Figure 7. The contribution (units: °C (100 km)$^{-1}$ month^{-1}) of the net heat flux term and its individual component to the GM tendency over the NPSTF from October to the following February: the net heat flux term (Qnet, blue), sensible heat flux term (Q_S, green), latent heat flux term (Q_L, red), longwave radiation term (Q_{LR}, purple), and shortwave radiation term (Q_{SR}, brown).

Figure 8. Same as Fig. 5c, except for the meridional temperature advection term calculated by the Ekman velocity.

Figure 9. Latitude-time sections of (a) the climatological monthly mean geopotential

height (shading; units: m^2 s^{-2}) and zonal wind speed at 1000 hPa (black contour; units: m s^{-1}), (b) the climatological monthly mean meridional ocean currents (units: m s^{-1}). All variables are averaged zonally over (140°E–170°W).

Figure 10. Meridional gradient of 10-m wind speed ($-\partial U_{10m}/\partial y$, black, units: 10^{-5} s^{-1}) and GM tendency calculated by the latent heat flux (Q_L, red, units: °C (100 km) $^{-1}$ $month^{-1}$) over the NPSTF. The blue curve (AL) is the latitude of climatological geopotential height at 900 m^2 s^{-2} averaged zonally over (140°E–170°W), representing the southward migration of the Aleutian low.

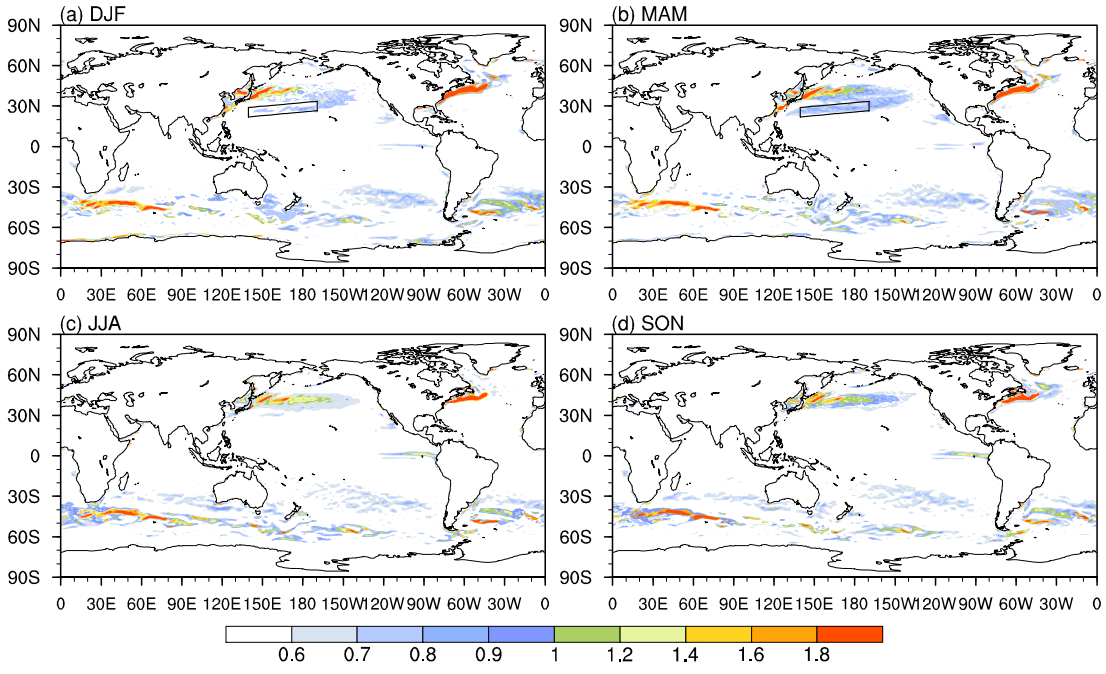

Figure 1. Climatological meridional SST gradients ($\left|\partial SST/\partial y\right|$, units: °C (100 km)$^{-1}$) in (a) winter, (b) spring, (c) summer, and (d) autumn. The winter refers to the time period of December in preceding year and January-February in the simultaneous year (DJF). The spring, summer and autumn refer to the time period of simultaneous March-Apil-May (MAM), June-July- August (JJA) and September-October-November (SON), respectively. The black boxes in (a) and (b) indicate the key area of the NPSTF.

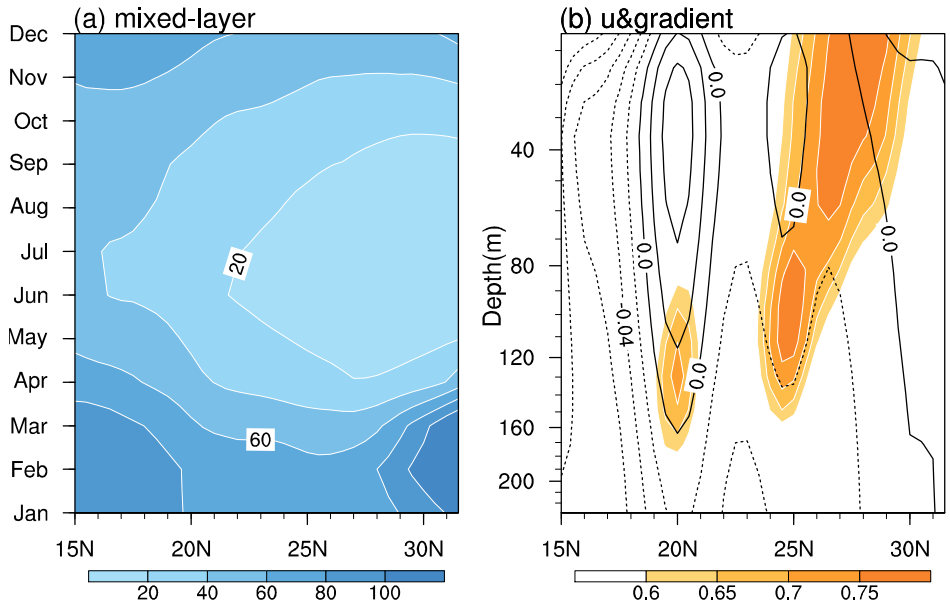

Figure 2. (a) Latitude-time section of the climatological monthly mean mixed-layer depth (units: m) calculated by $SST - T_H = 0.5°C$. (b) Latitude-depth section of the climatological zonal current velocity (black contour; units: m s^{-1}), superimposed with ocean temperature gradient (shading; units: °C (100 km) $^{-1}$); both are averaged over winter and spring. All three fields are averaged zonally over (140°E–170°W).

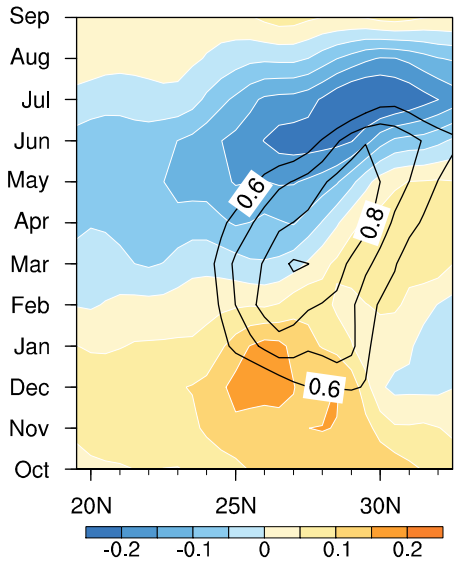

Figure 3. Latitude-time section of the climatological monthly mean gradient magnitude (GM) of the NPSTF (black contour; units: °C (100 km)$^{-1}$) and its tendency (shading; units: °C (100 km)$^{-1}$ month^{-1}), averaged zonally over (140°E–170°W).

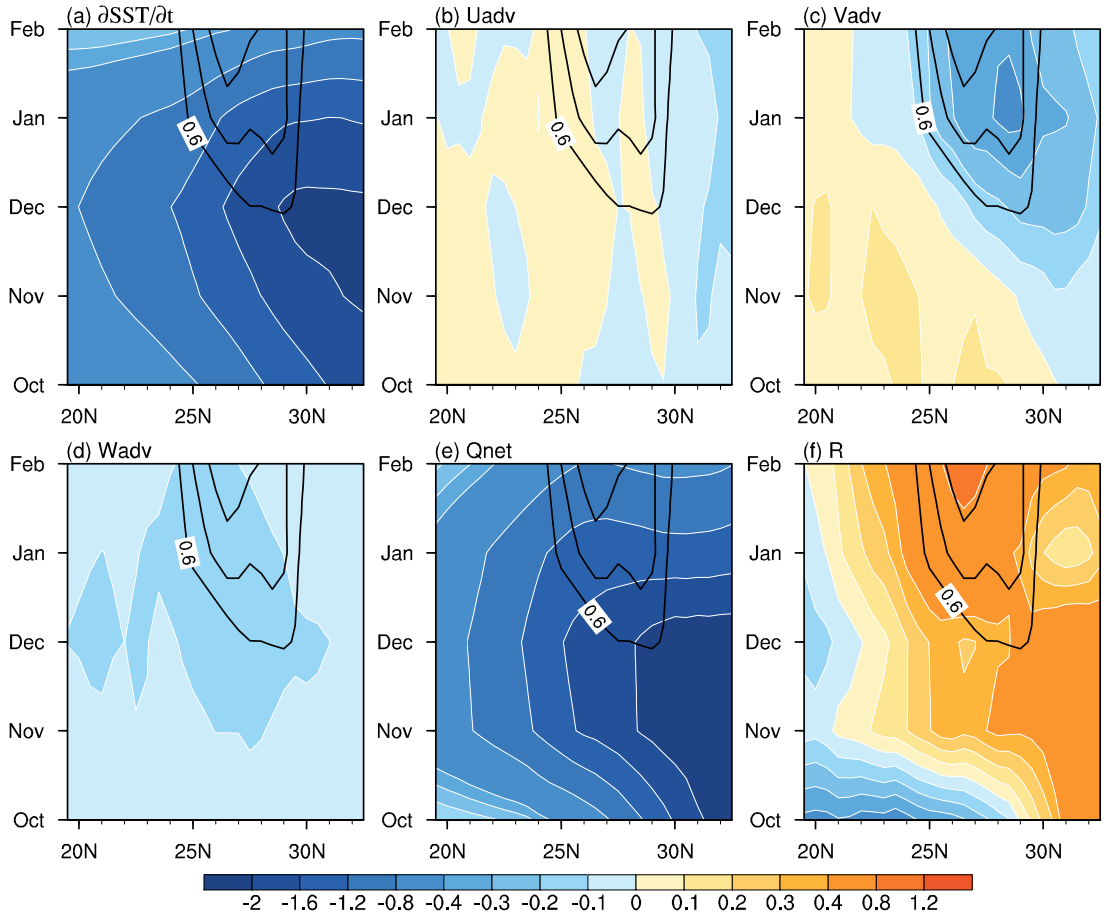

Figure 4. Latitude-time section of each term (shading; units: °C month^{-1}) in Eq. (1) from October to the following February, averaged zonally over (140°E–170°W). (a) shows the total SST tendency ($\partial SST/\partial t$), and (b–f) illustrate the components on the right-hand side of Eq. (1), namely, zonal temperature advection (Uadv), meridional temperature advection (Vadv), vertical temperature advection (Wadv), the net heat flux (Qnet), and the residual term (R). The black contours in each panel are the same, indicating the climatological monthly mean GM (units: °C (100 km)$^{-1}$), averaged zonally over (140°E–170°W).

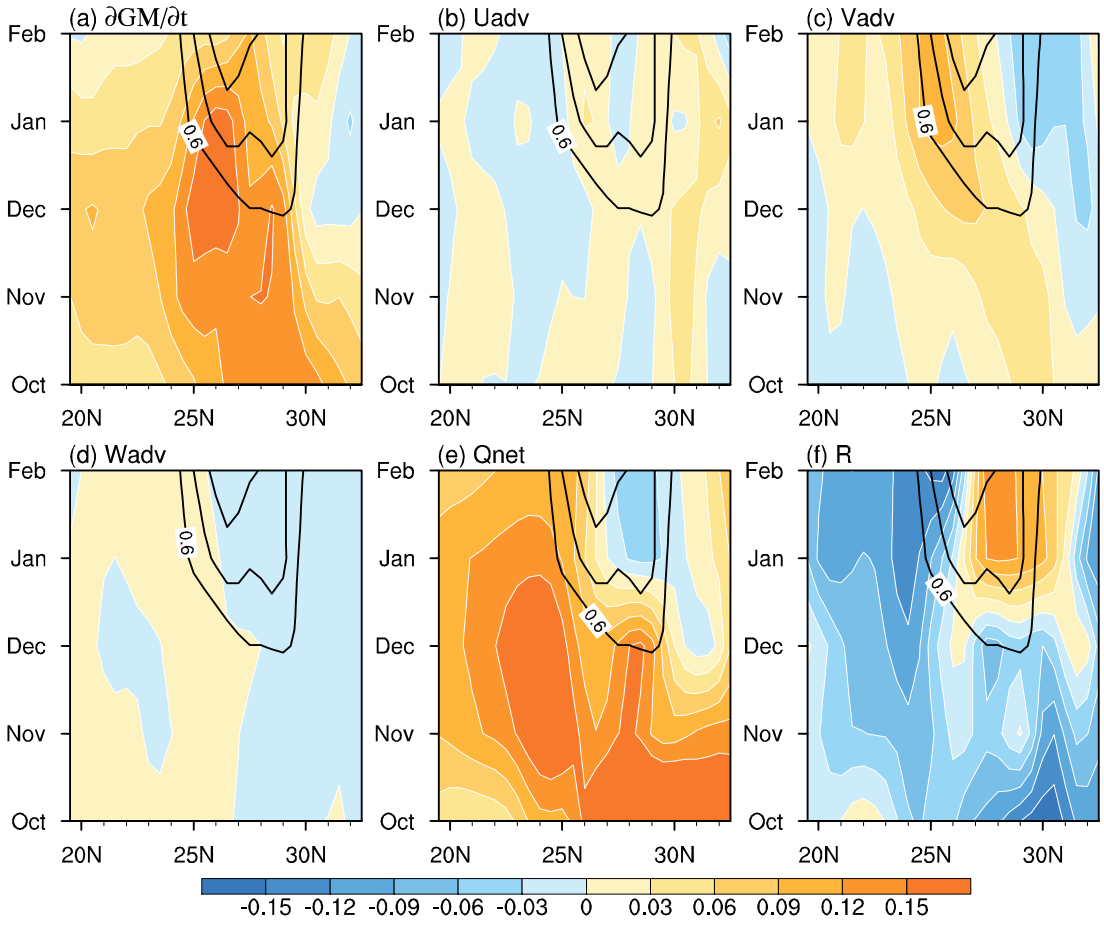

565

566 Figure 5. Same as Fig. 4, except for the terms (units: °C (100 km)$^{-1}$ month^{-1}) in Eq.

567 (2).

568

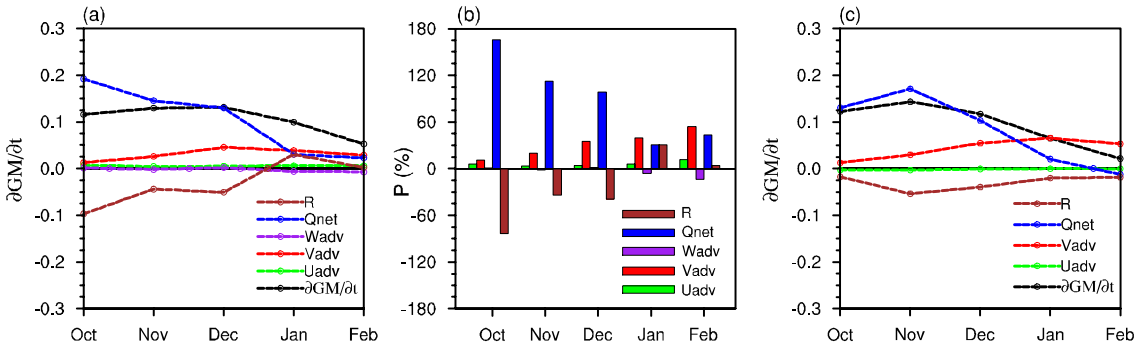

Figure 6. (a) The area mean GM tendency (units: °C (100 km) $^{-1}$ month^{-1}) over the NPSTF from October to the following February. (b) The contribution percentages (units: %) of the right-hand side terms in Eq. (2) to the left-hand side term. (c) Same as Fig. 6a, except using the Argo data from 2005 to 2013. The black dashed line in (a) and (c) is the GM tendency of the NPSTF. Green, red, purple, blue, and brown indicate zonal temperature advection (Uadv), meridional temperature advection (Vadv), vertical temperature advection (Wadv), the net heat flux (Qnet), and the residual term (R), respectively.

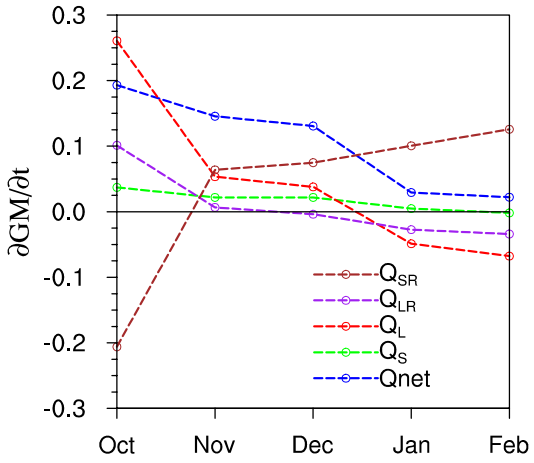

Figure 7. The contribution (units: °C (100 km) $^{-1}$ month^{-1}) of the net heat flux term and its individual component to the GM tendency over the NPSTF from October to the following February: the net heat flux term (Qnet, blue), sensible heat flux term (Q_S, green), latent heat flux term (Q_L, red), longwave radiation term (Q_{LR}, purple), and shortwave radiation term (Q_{SR}, brown).

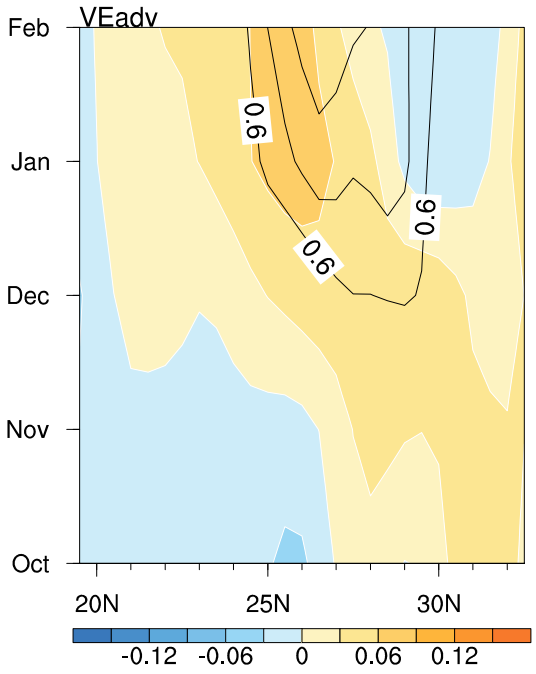

588

589 Figure 8. Same as Fig. 5c, except for the meridional temperature advection term

590 calculated by the Ekman velocity.

591

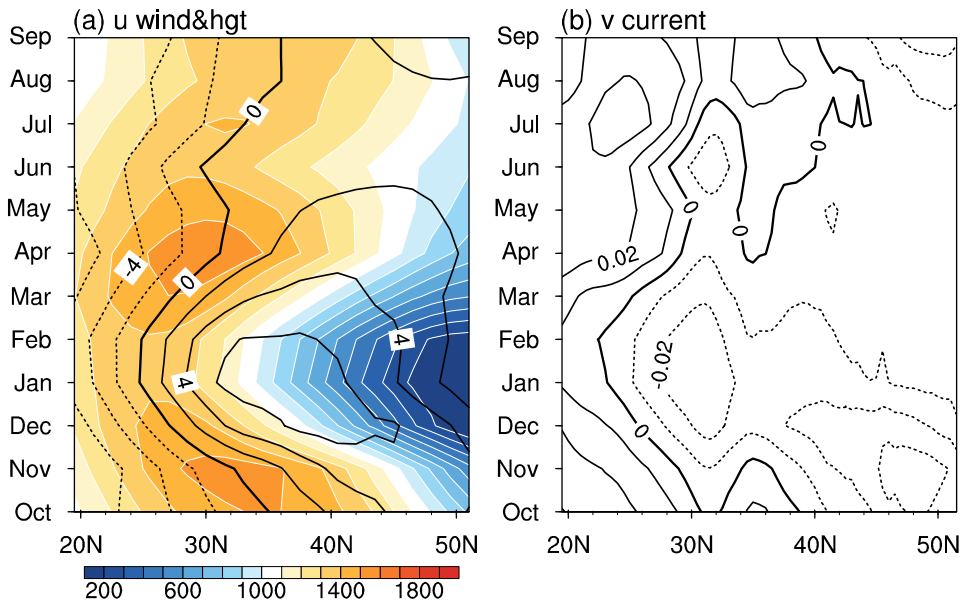

592

593 Figure 9. Latitude-time sections of (a) the climatological monthly mean geopotential

594 height (shading; units: m^2 s^{-2}) and zonal wind speed at 1000 hPa (black contour; units:

595 m s^{-1}), (b) the climatological monthly mean meridional ocean currents (units: m s^{-1}).

596 All variables are averaged zonally over (140°E–170°W).

597

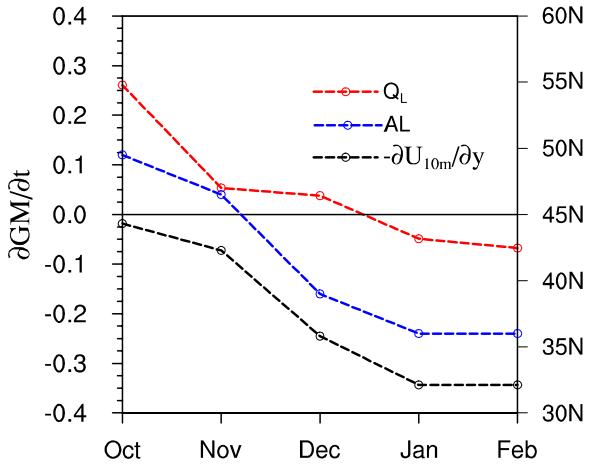

598

599 Figure 10. Meridional gradient of 10-m wind speed ($-\partial U_{10m}/\partial y$, black, units: 10^{-5} s^{-1})

600 and GM tendency calculated by the latent heat flux (Q_L, red, units: °C (100 km)$^{-1}$

601 month^{-1}) over the NPSTF. The blue curve (AL) is the latitude of climatological

602 geopotential height at 900 m^2 s^{-2} averaged zonally over (140°E–170°W), representing

603 the southward migration of the Aleutian low.

604